Enhanced capacity to CO_2 sorption in humid conditions with a K-doped biocarbon

Nausika Querejeta, Fernando Rubiera, Covadonga Pevida*

Instituto Nacional del Carbón, INCAR-CSIC, c/ Francisco Pintado Fe 26, 33011 Oviedo, Spain

*Corresponding author.

E-mail address: cpevida@incar.csic.es (C. Pevida)

Abstract

Solid sorbents with enhanced capacity and selectivity towards CO_2 are crucial in the design of an efficient capture process. Among the possible alternatives, K_2CO_3-doped activated carbons have shown high CO_2 capture capacity and rapid carbonation reaction rate. In this work, a sustainable and low-cost approach is developed with a biomass-based activated carbon or biocarbon as support. The CO_2 capture performance in cyclic sorption-desorption operation and the sorption kinetics have been investigated under different scenarios in a purpose-built fixed-bed set-up. Independently of the H_2O concentration in the flue gas, a constant relative humidity (~20%) in the K_2CO_3-doped biocarbon bed promoted the carbonation reaction and boosted the CO_2 sorption capacity (1.92 mmol/g at 50 °C and 14 kPa partial pressure of CO_2). Carbonation is slower than physical adsorption of CO_2 but wise process design could tune the operation conditions and balance capture capacity and sorption kinetics.

Keywords: Biocarbon; K_2CO_3; CO_2 sorption; Humid flue gas

1. Introduction

Carbon dioxide (CO_2) is the dominant greenhouse gas (GHG), accounting for at least 60% of all GHG emissions, and it is an essential component of the global carbon cycle [1]. CO_2 is produced in large quantities as a result of fossil fuel use in power generation and industry. Fossil fuel-fired power plants are the main source of carbon dioxide emissions worldwide, contributing to approximately 40% of total global emissions. Coal-fired power plants alone contribute to approximately 70% of the emissions from fossil fuel-fired power plants [2].

Therefore, it is becoming increasingly urgent to develop efficient carbon capture technologies for controlling the CO_2 emissions from fossil fuel combustion at point sources like, thermal power plants and steam generators. Post-combustion technologies

can be retrofitted to existing facilities and, therefore, are convenient to be deployed at large scale in a short time frame. Hence, post-combustion CO_2 capture can offer an interim solution for CO_2 removal from combustion flue gases, until new clean energy generation technologies emerge [3].

Under the low CO_2 partial pressure conditions found, for instance, in post-combustion flue gases the absorption/stripping process, using amine solutions such as monoethanolamine (MEA), is regarded as the most mature commercialized technology [4]. However, this technology presents several drawbacks that include high energy consumption, toxicity due to losses of the solvent, corrosion of the equipment, etc. Adsorption-based technologies for CO_2 capture entail a viable alternative due to their potential to be more energy efficient than chemical absorption.

In any adsorption-based process, adsorbate molecules are separated selectively from a gas mixture by means of a sorbent wherein the type of bonding involved depends on the pair adsorbate-sorbent. In this regard, CO_2 sorption can take place by means of physisorption, chemisorption, or even a mixture of both.

Flue gas from major CO_2 emitters contains less than 15 vol% CO_2 at temperatures above ambient and at atmospheric pressure. Non-CO_2 fraction composition is highly variable, although atmosphere gases are dominant. Water vapor, particularly, is a nuisance to capture CO_2 given the high concentration in the flue gas. It is therefore fair to say that most capture research efforts should be directed towards wet streams [1].

To accomplish the design of an efficient adsorption process it is mandatory to develop a proper adsorbent depending on the features of the gas streams to be treated. Designing an adsorbent for CO_2 capture under industrially acceptable standards focuses on the following attributes: (1) high CO_2 uptake, (2) high selectivity to CO_2, (3) cyclability over at least 1000 cycles, (4) fast kinetics, (5) stability in water vapor and acidic gases, and (6) the adsorbent should be produced at a low cost [1].

The capacity of conventional microporous adsorbents to adsorb CO_2 decreases in wet atmospheres and at temperatures higher than 40 °C, which makes their use inefficient [5]. At low pressures and in physisorption based solids, H_2O competes with CO_2 for the adsorption sites, leading to loss in uptake capacity [1].

Recently, it has been reported that dry regenerable alkali metal-based sorbents can be used to capture CO_2 in flue gas from fossil fuel-fired power plants [6]. In this context, water aids the capture of CO_2 by acting as a solvent and catalyst during bicarbonate formation. Thus, for such sorbents, both physisorption and chemisorption occur onto the surfaces of the sorbent and the alkali, respectively.

Among the various kinds of alkali metal-based sorbents [7–10], K_2CO_3 doped AC (activated carbon) has shown high CO_2 capture capacity and rapid carbonation reaction rate [11]. K_2CO_3 can capture CO_2 from flue gas at low temperatures (40–80 °C), forming potassium bicarbonate ($KHCO_3$) via the carbonation reaction [3]. Thus, it is very important to control the carbonation reaction rate and to tune the CO_2 absorption capacity of these sorbents in order to design a suitable dry regenerable sorbent for CO_2 capture [6].

With this regard, K_2CO_3 doped biomass-based AC is proposed herein as a promising candidate for CO_2 capture at low temperature (50 °C) under humid flue gas conditions. The use of a biomass-based activated carbon or biocarbon as support, scarcely reported in literature, constitutes a novel, sustainable and low-cost approach. To address the potentiality and applicability of the K-doped biocarbon produced, the CO_2 capture behaviors, performances in eight consecutive CO_2 sorption-desorption cycles, and sorption kinetics of both the AC support and the K_2CO_3/AC in a simulated flue gas atmosphere have been investigated in a purpose-built fixed-bed unit. Further insights have been focused into the effects of water pretreatment and the carbonation reaction pathways of K_2CO_3/AC for CO_2 capture.

2. Experimental

2.1. Sorbent preparation

Activated carbon RN2 previously produced in our laboratory departing from olive stones in a single-step CO_2 activation procedure [12] was selected as carbon support. This activated carbon is in granular form with average particle size of ~1–2 mm.

Anhydrous alkali metal carbonate, K_2CO_3 (Sigma Aldrich, ACS Reagent, ≥ 99.0%) was used as received for carbon impregnation. The dry potassium-based carbon sorbent was prepared through an impregnation method adapted from Guo et al. [13]. The preparation protocol was as follows: 5.0 g of activated carbon (RN2) were added to an aqueous solution containing 2.5 g of K_2CO_3 in 25 cm^3 of distilled water. It corresponds

to an impregnation ratio of 40% that has been identified as optimum [8]. Then, the content was mixed with a magnetic stirrer for 15 h at room temperature. After stirring, the mixture was dried in an air oven at 105 °C during 3.5 h. The dried sample was calcined in a furnace, at a slow heating rate of 5 °C/min up to 300 °C, under N_2 flow (100 cm^3/min) and a soaking time of 2 h was set. The resulting sample is named after RN2K, where K stands for the K_2CO_3 impregnation.

2.2. Sorbent characterization

2.2.1. Pore structure characteristics

The porous structure of the parent activated carbon (RN2) and the potassium-based carbon (RN2K) was assessed prior to the CO_2 sorption–desorption experiments. The porosity of the activated carbons was fully characterized by means of physical adsorption of N_2 at −196 °C, in a Micromeritics ASAP 2010, and adsorption of CO_2 at 0 °C, in a Micromeritics TriStar 3000. Helium density and apparent density were measured in an Accupyc 1330 at 35 °C and in a Micromeritics Autopore IV 9500 mercury porosimeter at 0.1 MPa, respectively. The samples were outgassed at 100 °C under vacuum overnight prior to all the measurements.

The use of both adsorbates, N_2 and CO_2, provides complementary information about the porous texture of the samples: the adsorption of CO_2 at 0 °C and up to atmospheric pressure is restricted to pores narrower than 1 nm, whereas N_2 adsorption at −196 °C covers wider pore sizes but presents diffusion limitations in the narrower pores. A summary of the methodology followed in the textural characterization is included in Table 1.

Table 1. Textural characterization performed from physical adsorption of N_2 at −196 °C and of CO_2 at 0 °C

Textural parameters		
Total pore volume	V_p	Amount of N_2 adsorbed at a relative pressure of 0.99
Surface area	BET	Brunauer-Emmett-Teller equation [14]
Micropore volume Micropore surface area	W_0 S_{DR}	N_2 isotherms: Dubinin-Radushkevich (DR) equation assuming a density of the adsorbed phase of 0.808 $cm^3\ g^{-1}$ and a cross sectional area of 0.162 nm^2 [15]; CO_2 isotherms: Dubinin-Astakhov (DA) equation assuming a density of the adsorbed phase of 1.023 $cm^3\ g^{-1}$ and a cross sectional area of 0.187 nm^2 [16]; E_0, characteristic energy, and n, exponent in the DA equation, only depends on the micropore system.
Average micropore width	L_0	Stoeckli-Ballerini equation [17]
Pore size distribution	PSD	Quenched Solid State (QSDFT) for N_2 isotherms and Non-local Density (NLDFT) Functional Theory for CO_2 isotherms, assuming slit pore model.

2.2.2. *Scanning electron microscopy (SEM)*

The success of the impregnation method and the distribution of K_2CO_3 onto the carbon precursor is another important parameter to be assessed. The particle morphology and composition of RN2K was examined by scanning electron microscopy with energy dispersive X-ray spectroscopy (SEM/EDX) in a Quanta FEG 650 equipped with an Ametek-EDAX analyzer (detector: Apollo X). The SEM images were taken at a magnification of 1500 and at 25 kV.

2.3. CO_2 sorption behavior of the sorbents

Single CO_2 sorption (breakthrough) and cyclic CO_2 sorption−desorption experiments of the studied solid sorbents were performed in a purpose-built fixed-bed unit thoroughly described elsewhere [18–23].

A simulated flue gas (total flowrate of 140 cm^3/min) composed of 14% CO_2, balance N_2, was fed to a bed at 50 °C and atmospheric pressure. Experiments in the presence of a stream of $H_2O_{(v)}$ (0.14 g/h) in addition to CO_2 and N_2 were also conducted in order to assess the role of water vapor in the CO_2 sorption process from flue gas.

The total flowrate (140 cm^3/min), pressure (130–140 kPa) and adsorption temperature (50 °C) were maintained constant in all fixed-bed experiments. Desorption

was carried out at 70 °C and applying a light vacuum of 10 kPa, simulating vacuum-temperature swing adsorption (VTSA) operation in the cyclic experiments.

The characteristics of the beds of the two carbons evaluated are presented in Table 2.

Table 2. RN2 and RN2K bed characteristics.

Bed Characteristics		RN2	RN2K
Mass of adsorbent	(g)	4.39	5.19
Total porosity	−	0.87	0.81
Helium density	(g/cm^3)	2.10	2.10
Apparent density	(g/cm^3)	0.50	0.72
Bed diameter	(cm)	1.30	1.30
Bed height	(cm)	11.90	10.00
Bed density	(g/cm^3)	0.28	0.39

2.3.1. *Cyclic fixed-bed operation*

CO_2 sorbents should be easy to regenerate and should keep its performance with cycling. Thus to evaluate the performances to separate CO_2 from simulated flue gas streams over multiple cycling, the activated carbons (ACs) were subjected to eight consecutive sorption-regeneration cycles. Each experimental run involved the following steps: preconditioning, sorption and regeneration. A detailed description is presented elsewhere [23].

Humidity contained in the flue gases negatively affects the CO_2 adsorption capacity of ACs due to their high affinity to moisture; however, the presence of water vapor is essential to form potassium bicarbonate from dry regenerable alkali metal-based sorbents upon reaction with CO_2 [24]. Thus, a different mechanism of interaction with CO_2 is expected for the two activated carbons under evaluation, particularly when assessed in wet conditions. To study the influence of water vapor in CO_2 sorption and evaluate the stability of the performances, RN2 and RN2K were subjected to other eight consecutive sorption–desorption cycles. The experimental runs included the same steps as in the dry cases but during the adsorption step a ternary mixture consisting of 14% CO_2/ 84% N_2/ 2% H_2O was fed to the bed [23].

It is important to note that before each experiment the sorbent bed was dried by flowing N_2 (140 cm^3/min) for 60 min at 150 °C and atmospheric pressure.

2.3.2. *Breakthrough experiment in water vapor pre-saturated bed*

As explained above in Section 2.3.1 the presence of moisture in the flue gas stream leads to a decrease in the CO_2 adsorption capacity of an activated carbon due to co-adsorption of H_2O but it is mandatory to the carbonation process of dry regenerable alkali metal-based sorbents. Therefore, to evaluate the effect of H_2O on CO_2 sorption performance, breakthrough non-cyclic experiments feeding a ternary gas mixture composed of 14% CO_2/ 84% N_2/ 2% H_2O were carried out over extended time (several hours) till saturation of the bed with H_2O.

Since high concentrations of water vapor are beneficial for improving the carbonation reaction activity, a way suggested to reach effective CO_2 sorption performance is to increase the carbonation conversion and reaction kinetics including water pretreatment prior to CO_2 sorption [25,26]. To investigate the effect of this pretreatment, the bed was initially saturated with H_2O by feeding a gas stream containing 98% N_2 and 2% H_2O. Afterwards, ternary $CO_2/N_2/H_2O$ breakthrough curves (non-cyclic experiments) were obtained similarly to the long experiments with a fresh bed.

2.4. Theory/calculation

The design of a sorption process is not fully addressed with equilibrium data; sorption kinetics are also required.

2.4.1. CO_2 adsorption kinetics

In physical-based sorption, commonly denoted as adsorption, diffusion of adsorbate molecules into the adsorbent particles is the rate controlling step.

To describe the adsorption process quantitatively and identify the adsorption mechanism, a number of adsorption kinetic models have been developed [27]. Based on a previous work [28], two models will be considered herein to describe the CO_2 adsorption behavior of RN2 and RN2K under the different moisture conditions evaluated: pseudo-first-order [29] and Avrami´s fractional [30] models.

Table 3 shows the list of equations associated to these kinetic models, where *t* is the time elapsed from the beginning of the adsorption process, q_t (mmol/g) is the amount adsorbed at a given time, q_e (mmol/g) represents the amount adsorbed at equilibrium, k_f (min^{-1}) is the pseudo-first-order rate constant, k_A (min^{-1}) is the Avrami's kinetic constant and n_A is the Avrami's exponent.

Table 3. Adsorption kinetics models.

Kinetic model	Equation	Differential form
Pseudo-first order	$q_t = q_e(1 - e^{-k_f t})$	$\frac{dq_t}{dt} = k_f\,(q_e - q_t)$
Avrami	$q_t = q_e(1 - e^{(-(k_A t)^{n_A})})$	$\frac{dq_t}{dt} = {k_A}^{n_A}\, t^{n_A - 1}(q_e - q_t)$

Furthermore, to measure the discrepancy between the measured data and the predictions from the model, the sum of squared errors (SSE) [25] and the coefficient of determination (R^2) [27,28] were estimated. Equations are shown in Table 4, where $\boldsymbol{q_{t,exp}}$ and $\boldsymbol{q_{t,pred}}$ are the experimentally measured and model-predicted adsorption capacities, respectively, N is the number of experimental data points for each sample and p is the number of parameters of the model.

Table 4. Goodness of fitting of the kinetic models equation.

Sum of squared errors (SSE)	$\mathrm{SSE}(\%) = \sqrt{\frac{\sum(q_{t,exp} - q_{t,pred})^2}{N}} \times 100$
Coefficient of determination (R^2)	$R^2 = 1 - \left(\frac{\sum_{i=1}^{N}(q_{t,exp} - q_{t,pred})^2}{\sum_{i=1}^{N}(q_{t,exp} - \overline{q_{t,exp}})^2}\right)\left(\frac{N-1}{N-p}\right)$

2.4.2. CO_2 sorption kinetics

CO_2 capture on potassium-based sorbents is more likely to be a chemical-sorption based process, which involves the reaction with CO_2 to form bicarbonate. During this sorption process, adsorption and carbonation co-exist [7]; diffusion of CO_2 to the surface and into the pores, reaction with the active sites and formation of a layer of compact products are the main steps [25]. Thus, with the aim of studying the kinetics of CO_2 sorption on RN2K, the Shrinking Core Model (SCM) was adopted to correlate the experimental data [31]. The basis of the SCM establishes that the solid is non-porous and it is initially surrounded by a fluid film through which mass transfer occurs between the solid particle and the bulk of the fluid. As the reaction proceeds, a layer of product (i.e., potassium bicarbonate) forms around the unreacted core. The solid particle is assumed to be spherical and it reacts with the fluid isothermally. Besides, the concentration of the reacting fluid is supposed to be constant or in excess [32].

Table 5 shows the list of equations associated to the SCM when applied to CO_2 sorption on K_2CO_3 doped materials, where q (mmol/g) is the total amount of CO_2 captured, q_p (mmol/g) is the amount of physically adsorbed CO_2 at a given time, $M_{K_2CO_3}$ is the molecular mass of K_2CO_3 (g/mol), β represents the K_2CO_3 loading in the sorbent (being 1 for pure potassium carbonate), R (cm) is the radius of the particle, k_s is the reaction rate constant per unit of reaction interface, $C^0{}_{CO_2}$ (mmol/cm^3) and $C^0{}_{H_2O}$ (mmol/cm^3) are the initial concentrations of CO_2 and H_2O, respectively, $C^0{}_{K_2CO_3}$ (mmol/cm^3) is the initial concentration of K_2CO_3 and D_e is the diffusion coefficient for H_2O in the product layer. The specific derivation of the expression can be found elsewhere [31].

Table 5. Shrinking core model equations.

Parameters	Equation
Carbonation conversion of the sorbent	$\eta = \frac{(q - q_p) \times M_{K_2CO_3}}{\beta \times 1000} \times 100\%$
Global reaction rate	$t = \frac{R}{k_s C^0{}_{CO_2} C^0{}_{H_2O}}(1-(1-\eta)^{\frac{1}{3}}) + \frac{C^0{}_{K_2CO_3} R^2}{6 D_e C^0{}_{H_2O}}(1-3(1-\eta)^{\frac{2}{3}} + 2(1-\eta))$
Surface chemical reaction-controlled region	$t = A_1\, g(\eta)$ $g(\eta) = 1-(1-\eta)^{\frac{1}{3}}$ $A_1 = \frac{R}{k_s C^0{}_{CO_2} C^0{}_{H_2O}}$
Internal diffusion-controlled region	$t = A_2\, P(\eta)$ $P(\eta) = 1-3(1-\eta)^{\frac{2}{3}} + 2(1-\eta)$ $A_2 = \frac{C^0{}_{K_2CO_3} R^2}{6 D_e C^0{}_{H_2O}}$

3. Results and discussion

3.1. Adsorbents characterization

3.1.1. *Pore structure characteristics*

The N_2 adsorption isotherms at −196 °C of the carbons are shown in Fig. 1(a). Both activated carbons presented type I adsorption isotherms, according to IUPAC

classification, characteristic of microporous materials. As previously explained elsewhere [12], from the open elbow in the low pressure range of the N_2 adsorption isotherm on RN2, it is deduced that this activated carbon possesses both narrow and wider microporosity. Wider micropore size distribution is suitable to impregnate an activated carbon. On the other hand, RN2K shows an isotherm with a slightly sharper elbow than RN2 that suggests narrower pore size distribution (PSD). Moreover, micropore size distribution slightly shifts to smaller micropores after impregnation (see Fig. 1b).

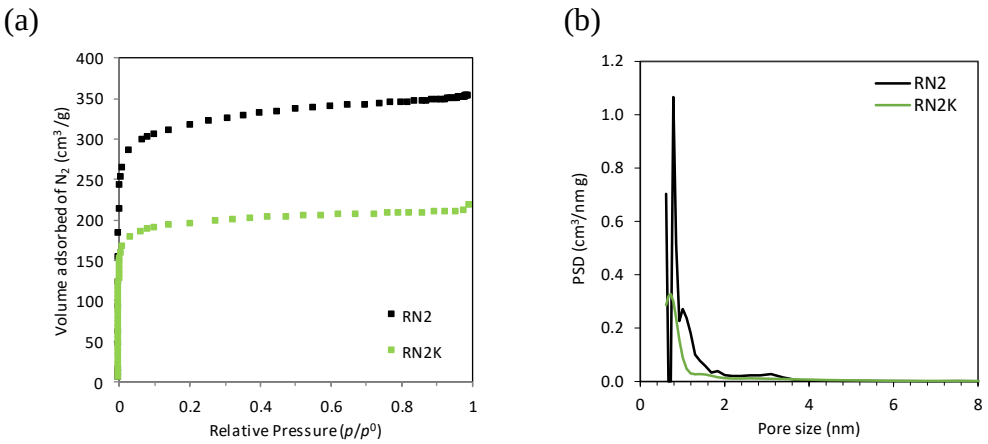

Fig. 1. (a) N_2 adsorption isotherms at −196 °C and (b) N_2 adsorption QSDFT PSD of RN2 ACs.

The CO_2 adsorption isotherms of the samples at 0 °C are represented in Fig. 2(a). Comparison of the volumes adsorbed of both adsorbates, N_2 and CO_2, gives an indication of the micropore ratio in each sample. Both activated carbons show similar PSD in the narrow microporosity domain (Fig. 2b). Table 6 summarizes the textural parameters estimated from the adsorption isotherm data.

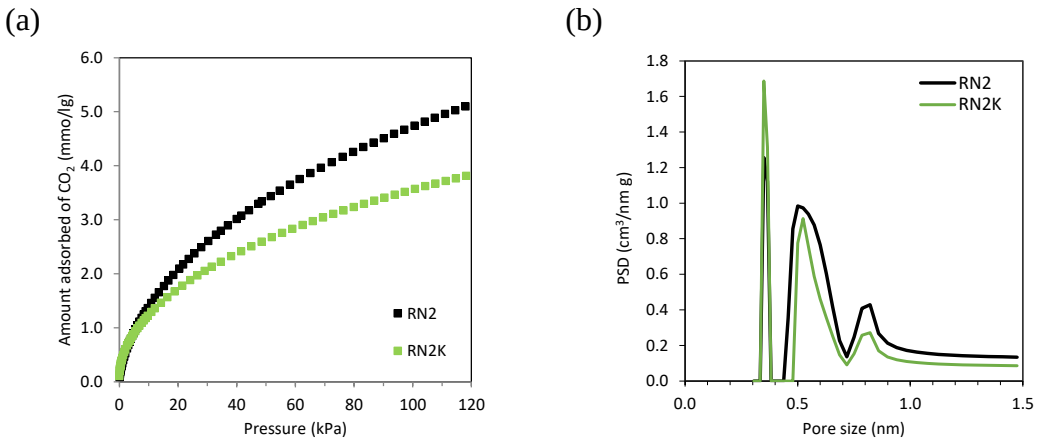

Fig. 2. (a) CO_2 adsorption isotherms at 0 °C and (b) CO_2 adsorption NLDFT PSD of RN2 ACs.

The impregnation of RN2 with potassium carbonate notably reduces the volume of available porosity for N_2 and CO_2 adsorption. Micropore surface areas (S_{mi}) estimated from both N_2 and CO_2 isotherms decrease 26% and 22%, respectively, while reduction in micropore volumes (W_0) accounts for 37% and 32%, respectively.

RN2K shows an average narrow micropore size of 0.69 nm, which has been pointed out as very suitable for CO_2 adsorption at post-combustion capture conditions [33–39]. However, even though it has been demonstrated that pore size governs CO_2 adsorption at low pressures [33–37], the reduction of the narrow micropore volume ($W_{0,CO2}$) certainly penalizes the adsorption of CO_2 on RN2K.

Table 6. Textural parameters of the RN2 ACs as estimated from the N_2 and CO_2 adsorption isotherms.

Sample	N_2 Adsorption (−196 °C)						CO_2 Adsorption (0 °C)				
	V_p [1]	S_{BET} [2]	W_0 [1]	E_0 [3]	L_0 [4]	S_{mi} [2]	n	W_0 [1]	E_0 [3]	L_0 [4]	S_{mi} [2]
RN2	0.53	1248	0.48	21.3	1.09	888	1.7	0.44	24.9	0.80	1112
RN2K	0.34	768	0.30	23.1	0.92	657	1.6	0.30	27.0	0.69	868

[1] V, W in cm^3/g; [2] S in m^2/g; [3] E_0 in kJ/mol; [4] L_0 in nm.

Therefore, it can be inferred that impregnation with K_2CO_3 tends to block the porosity of the parent carbon to some extent, reducing notably the capacity to adsorb N_2 and CO_2. This blockage largely occurs on the wider micropores (see Fig. 1b) and it has been attributed by Hayashi et al. [8] to the hydrophobicity of the carbon surface that repels droplets of aqueous potassium carbonate that move toward the wider end of the pore space.

3.1.2. Scanning electron microscopy (SEM)

To gather more insights into the characteristics of RN2K it was analyzed by SEM/EDX to assess the effect of impregnation with K_2CO_3.

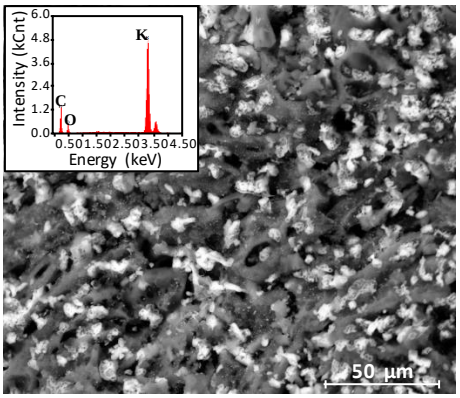

Fig. 3. SEM image of the impregnated carbon RN2K.

Fig. 3 shows the morphology of RN2K characterized by small white aggregates with average sizes of less than 10 µm that are homogeneously dispersed in the carbon structure. These white aggregates correspond to K_2CO_3 as confirmed by EDX analysis (inset in Fig. 3). EDX shows high intensity potassium peak in carbon RN2K but also indicates the presence of lower intensities of C and O in the sorbent.

3.2. CO_2 sorption performance of the RN2 ACs

3.2.1. Cyclic fixed-bed operation

Stability of a CO_2 sorbent in long-term cyclic operation is crucial. Thus to evaluate the performances of RN2 and RN2K in multiple cycle operation, different scenarios were considered: separation of CO_2 from CO_2/N_2 and from $CO_2/N_2/H_2O$ gas streams. The CO_2 sorption capacities of RN2 and RN2K during 8 consecutive cycles of sorption-regeneration were compared. The sorbents were allowed to reach CO_2 saturation (maximum sorption capacity) during the sorption step and they were practically fully regenerated during the desorption step. Under humid conditions, H_2O sorption was also evaluated.

A mass balance was applied to the bed in each sorption–desorption cycle to calculate the specific amount of CO_2 retained in the bed and the holdup of the gas phase was discounted applying correction factors. Detailed information about the calculation procedure can be found in ref. [19]. H_2O sorption is significantly slower than CO_2; however, a similar calculation procedure was followed to estimate the total amount of H_2O uptake at the time when the bed reached saturation in CO_2.

Fig. 4 plots the CO_2 and H_2O adsorption capacities of RN2 for the eight consecutive cycles during the binary (CO_2/N_2) and ternary ($CO_2/N_2/H_2O$) experiments.

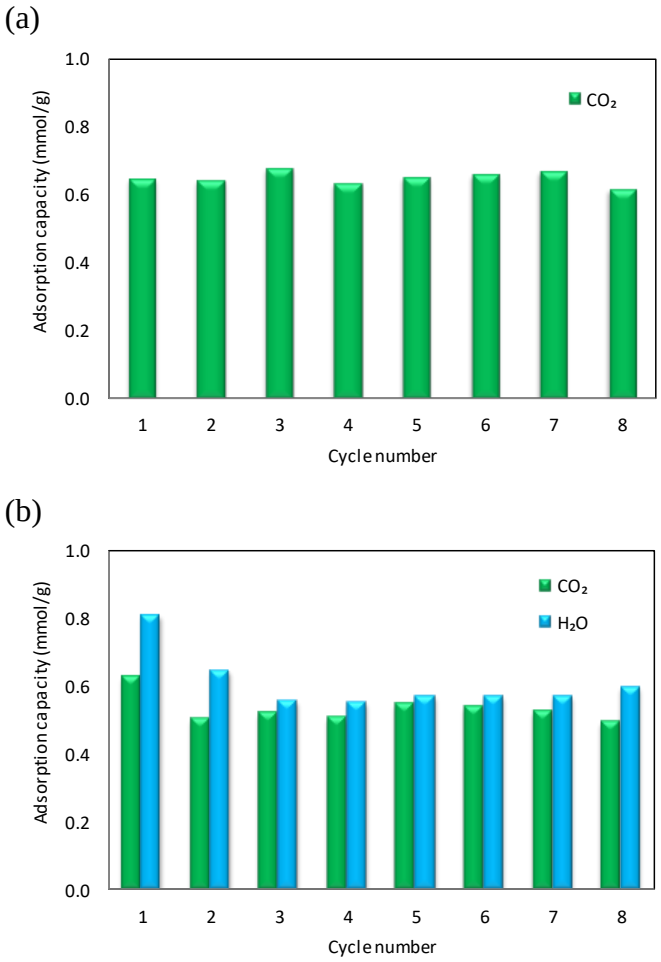

Fig. 4. Adsorption capacities of RN2 in multiple cycles: (a) CO_2/N_2 and (b) $CO_2/N_2/H_2O$ experiments.

As can be seen from Fig. 4(a), the CO_2 adsorption capacity of RN2 is maintained over the eight consecutive cycles (0.65 mmol/g in cycle 1 and 0.62 mmol/g in cycle 8), indicating that the sorbent keeps considerable long-term working stability and cyclability. The same trend is observed for H_2O adsorption (Fig. 4b) with the exception of the first cycle. It has to be borne in mind that the bed is fully regenerated at the beginning of the first cycle and H_2O adsorption and desorption are significantly slower. This implies that H_2O is not fully removed from the bed at the beginning of each intermediate cycle. Thus, for comparative purposes among the different experiments, the capture capacity was evaluated hereafter as an average of the sorption performance over the last five cycles (cycles 4 to 8) in which concentrations of both CO_2 and H_2O can be considered stable [23]. Results are shown in Table 7 for samples RN2 and RN2K.

Table 7. CO_2 and H_2O sorption capacities (average 4–8 cycles)

Sample	Feed gas	CO_2 sorption capacity (mmol/g)	H_2O sorption capacity (mmol/g)
RN2	CO_2/N_2	0.63	–
	$CO_2/N_2/H_2O$	0.52	0.53
RN2K	CO_2/N_2	0.50	–
	$CO_2/N_2/H_2O$	0.41	0.53

Despite the doping with potassium carbonate, sample RN2K exhibits a much lower CO_2 uptake (reduction of 21% on average for the experiments under dry and wet conditions) when compared to RN2. This could be expected for the experiments in dry conditions where the textural properties of the carbon play a significant role, due to prevalence of physical adsorption, and the impregnated sample needs to offset the substantial reduction in micropore volume. However, the sorption capacities from the ternary experiments ($CO_2/N_2/H_2O$) revealed that the presence of moisture penalized the CO_2 uptakes of both carbons similarly. This phenomenon could be a result of the combination of the following two factors: the different kinetics of sorption of CO_2 and H_2O and, most importantly, the absence of carbonation reaction due to a low H_2O/CO_2 ratio (1:6) [6] or to insufficient relative humidity during the cycles [11,38]. For this reason, further experiments were conducted in the presence of water vapor to gain more insights into the role of water vapor on CO_2 sorption on RN2K.

3.2.2. Breakthrough experiments in humid conditions

To assess the effect of H_2O concentration on carbonation, breakthrough experiments were carried out over extended time (several hours) feeding a ternary mixture composed of 14% CO_2, 84% N_2 and 2% H_2O to the bed at 50 °C and atmospheric pressure. These non-cyclic experiments departed from a fully regenerated sorbent and reached saturation of the bed with H_2O.

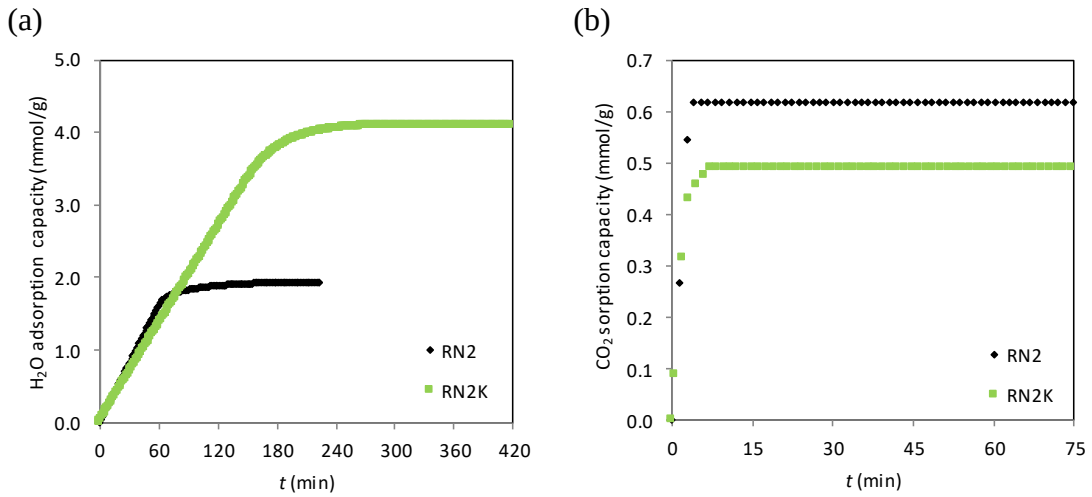

Fig. 5. H_2O (a) and CO_2 (b) sorption capacities for RN2 and RN2K during breakthrough experiments.

As can be seen in Fig. 5(a), the H_2O profiles took longer times to break through the bed: 60 and 148 min for RN2 and RN2K, respectively. This difference in adsorption time is translated into larger H_2O sorption capacities for the potassium carbonate based sorbent RN2K (113% greater capacity than RN2, see Table 8).

Despite the sharp increase in H_2O uptake, CO_2 broke through the bed in the first minutes of the experiment (~ 2 min), as can be observed in Fig. 5(b), and the CO_2 sorption capacities remained unaltered for both carbons, showing the same value as that previously reported for cycle 1 of the multiple cycle experiments with a ternary gas mixture (Table 8).

Table 8. CO_2 and H_2O sorption capacities in humid breakthrough experiment.

Sample	CO_2 sorption capacity (mmol/g)	H_2O sorption capacity (mmol/g)
RN2	0.62	1.92
RN2K	0.49	4.09

This result corroborates the performance of the parent carbon RN2 in multiple cycling, where only physical adsorption of CO_2 was observed. However, a different pattern would have been expected for the potassium carbonate based sorbent, RN2K, given that the bed was allowed to reach saturation in H_2O.

Chemical sorption of CO_2 on potassium carbonate based solid sorbents rely on the carbonate as the active phase to form potassium bicarbonate ($KHCO_3$) through the following carbonation reaction (1):

$$K_2CO_3(s) + H_2O(g) + CO_2(g) \leftrightarrow 2KHCO_3(s) \quad (1)$$

However, CO_2 sorption does not take place straightaway via reaction 1, the following reaction steps may coexist [39]:

$$K_2CO_3(s) + 1.5H_2O(g) \leftrightarrow K_2CO_3 \cdot 1.5H_2O(s) \quad (2)$$

$$K_2CO_3 \cdot 1.5H_2O(s) + CO_2(g) \leftrightarrow 2KHCO_3(s) + 0.5H_2O(g) \quad (3)$$

$$2K_2CO_3(s) + 2.5H_2O(g) + CO_2(g) \leftrightarrow K_4H_2(CO_3)_3 \cdot 1.5H_2O(s) \quad (4)$$

$$K_4H_2(CO_3)_3 \cdot 1.5H_2O(s) + CO_2(g) \leftrightarrow 2KHCO_3(s) + 0.5H_2O(g) \quad (5)$$

Jayakumar et al. [3] have confirmed that the carbonation and hydration reactions of K_2CO_3 (Eqs. 1 and 2, respectively) occur as competing reversible and parallel reactions in a simulated flue gas atmosphere, whilst reaction (3) does not occur or is negligible. In reaction (4), $K_4H_2(CO_3)_3 \cdot 1.5H_2O(s)$ is an additive combination or a partial dissolution of $2KHCO_3(s)$ in $K_2CO_3 \cdot 1.5H_2O(s)$ that requires both H_2O and CO_2 to form.

On the other hand, it has been previously reported that the CO_2 concentration has much lesser effect on the carbonation reaction paths than the H_2O concentration [6,11,40]. Zhao et al. reported that the carbonation rate for $K_4H_2(CO_3)_3 \cdot 1.5H_2O(s)$ is higher than that of $K_2CO_3 \cdot 1.5H_2O(s)$ and so the hydration reaction is considered as the rate-controlling step for the CO_2 sorption process [11,41]. Moreover relative humidity in the bed plays a very important role, it needs to reach a sufficient level to prevent the reversal transformation of the active species to the original phase, K_2CO_3 [11,26].

Taking into consideration the aforementioned, the theoretical water uptake as per 1 g of RN2K calculated from Eq. (1) is 4.44 mmol/g. The experimental water uptake calculated from the breakthrough experiments reached 4.09 mmol/g where 1.59 mmol/g might correspond to physical adsorption of water on RN2K. The latter value is calculated departing from the uptake of the parent carbon RN2 (see Table 8) and subtracting the water vapor adsorption difference between RN2 an RN2K (~ 17%) as estimated from the first cycle of the wet cyclic experiments. Hence around 2.50 mmol/g of H_2O represent the amount of water available to convert K_2CO_3 into the intermediate $K_2CO_3 \cdot 1.5H_2O(s)$. This value only accounts for half (56%) of the theoretical value and, consequently, it may be insufficient to allow $K_4H_2(CO_3)_3 \cdot 1.5H_2O(s)$ formation (Eq. (4)).

During the breakthrough non-cyclic experiment, the relative humidity does not remain constant. It increases up to saturation of the bed in H_2O and so does the water

uptake. The maximum relative humidity achieved in the gas phase was around 20%. For approximately 160 min, the relative humidity in the gas exiting the RN2K bed is negligible due to H_2O being mainly adsorbed on the bed (See Fig. 6). The unavailability of water vapor hinders the hydration reaction, which is the rate limiting step, and so the carbonation process does not take place.

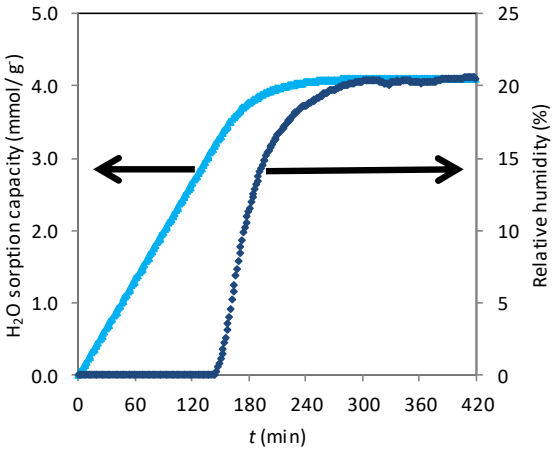

Fig. 6. Relative humidity and H_2O sorption capacity profiles on RN2K.

Thus, we can conclude that due to the low values of H_2O concentration in the feed gas (2 vol%) and the low relative humidity in the bed during the experiment, the carbonation reaction in the RN2K bed was hindered during the breakthrough experiments. This conclusion is in agreement with Lee et al. [24], that attributed the deficient conversion of K_2CO_3 into $K_2CO_3 \cdot 1.5H_2O(s)$ to the low H_2O concentration and to the equilibrium of absorption and desorption of water at low relative humidity.

3.2.3. Effect of water vapor pre-saturation of the bed on CO_2 sorption

As explained in the previous section, carbonation of potassium carbonate based sorbents proceeds through two main steps: firstly hydration reaction occurs to form $K_2CO_3 \cdot 1.5H_2O(s)$ (rate-controlling) and/or $K_4H_2(CO_3)_3 \cdot 1.5H_2O(s)$ under moist conditions and, secondly, the intermediates react with CO_2 to form $KHCO_3$. Hence, to investigate the effect of water pretreatment on the CO_2 sorption performances of both activated carbons, ternary $CO_2/N_2/H_2O$ breakthrough non-cyclic experiments were conducted departing from beds initially saturated with H_2O and N_2. The H_2O and CO_2 sorption capacity profiles are plotted in Figures 7a and 7b.

H_2O sorption process follows the same pattern observed in the experiments with a fully regenerated fresh bed (see Fig. 5). However, it is apparent that the H_2O uptakes are enhanced for the two carbons due to the absence of CO_2 during the saturation stage that thereby avoids competitive adsorption. It can be noted that the H_2O capture capacity for RN2K has increased very significantly given that the bed took around 1000 min to reach saturation. On the other hand, the trend in CO_2 sorption reversed with respect to the fresh bed breakthrough experiments: the adsorption capacity of RN2 is reduced due to co-adsorption of H_2O but in the case of RN2K, conditions seem to favor chemical sorption of CO_2 and a significant enhancement in the CO_2 uptake is observed. Thus, under these conditions of saturation in water, RN2K outperforms RN2.

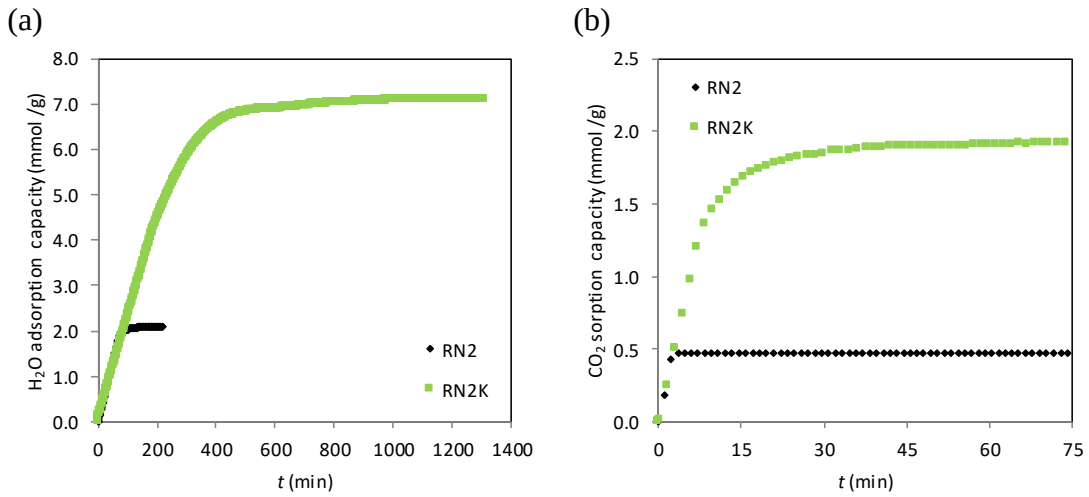

Fig. 7. H_2O (a) and CO_2 (b) sorption capacities for RN2 and RN2K with water vapor pre-saturation of the bed.

Physical adsorption of water (calculated as explained in section 3.2.2) on RN2K accounts for 1.73 mmol/g. As the theoretical value for water absorption as per 1 g of RN2K is 4.44 mmol/g and the total sorption capacity of the potassium based carbon is 7.09 mmol/g (see Table 9), there is a 13% excess water. Thus, it can be deduced that the potassium carbonate present in RN2K has been converted to $K_2CO_3 \cdot 1.5H_2O$ [11,26,39].

Table 9. H_2O and CO_2 sorption capacities in saturated beds.

Sample	CO_2 sorption capacity (mmol/g)	H_2O sorption capacity (mmol/g)
RN2	0.47	2.09
RN2K	1.92	7.09

The CO_2 adsorption capacity of RN2 has reduced in a 24% with regards to the experiment without pretreatment (Section 3.2.2). The CO_2 capture capacity of RN2K rapidly increased to 1.72 mmol/g (~17 min) and then slowly approached the maximum value of 1.92 mmol/g. This means that the vast majority of the sorption capacity of RN2K at these conditions relies on chemisorption in the K_2CO_3 phase. In amine scrubbing processes where a solution with 30 wt.% monoethanolamine (MEA) is frequently used [42–45], CO_2 absorption capacity expressed as the difference between rich and lean solvent loadings is of about 1.23 mmol CO_2/g solution [42,43]. Thus, the uptake capacity of RN2K surpasses in around 56% the outstanding capacity attributed to chemical absorption in amine-based solvents. Regarding other K-based sorbents, Lee et al. [26,46,47] attained a CO_2 capture capacity of 1.95 mmol/g for sorbent KACI30 at 60 °C (feed gas composition: 9 vol% H_2O, 1 vol% CO_2) whilst Guo et al. [25] obtained a CO_2 uptake of 1.18 mmol/g for KACI15 at 20 °C (feed gas composition: 2 vol% H_2O, 1 vol% CO_2). Even though the testing conditions selected in these works differ from those in this study, the reported CO_2 uptakes corroborate the great performance of RN2K.

Despite that the H_2O concentration is not changed in the two sets of breakthrough experiments (2 vol% H_2O in the feed gas for both the fresh and the pre-saturated bed experiments), the reason for the existence of carbonation is that water vapor pretreatment increases the relative humidity in the bed of RN2K up to 20% and this value remains constant from the beginning of the experiment whilst CO_2 sorption is taking place. With water vapor pretreatment, the relative humidity in the bed is enough to allow hydration of K_2CO_3 to $K_2CO_3 \cdot 1.5H_2O$. In environments of extremely high relative humidity K_2CO_3 will be more likely to be converted into $K_4H_2(CO_3)_3 \cdot 1.5H_2O$ during the carbonation process as shown in Eq. (4) [11,24,26,48,49]. Thus, controlling water pretreatment is crucial in the performance of RN2K as CO_2 sorbent: once $K_2CO_3 \cdot 1.5H_2O$ is formed, the relative humidity needs to be high enough to prevent the transformation back from $K_2CO_3 \cdot 1.5H_2O$ to the original phase, K_2CO_3, and to proceed with the carbonation reaction.

3.3. Volumetric CO_2 uptake capacity

The foregoing discussion evidences that the potassium carbonate based carbon RN2K shows an outstanding CO_2 performance under conditions of saturation in H_2O; meanwhile RN2 shows better behavior in dry conditions. CO_2 uptakes were reported in mass basis but it is nevertheless important to address them in volume basis, especially for

post-combustion capture applications wherein reduction of the carbon footprint is a major challenge. In such scenario, the CO_2 uptake per given space (volume) occupied by the adsorbent (i.e., volumetric uptake) must be maximized [38]. CO_2 volumetric capacities of both activated carbons have been calculated departing from the uptake capacities presented previously and the bed densities shown in Table 2.

Table 10. CO_2 volumetric capacities of the support RN2 and the impregnated sample RN2K when feeding $CO_2/N_2/H_2O$ to the bed.

Sample	Experiment	Bed initial conditions	CO_2 volumetric capacity (mmol/cm^3)
RN2	Multicycle, average 4-8	Fresh bed-not fully regenerated in cycling	0.14
	Breakthrough experiment	Fresh bed-H_2O saturation	0.17
		Water pretreatment	0.13
RN2K	Multicycle, average 4-8	Fresh bed-not fully regenerated in cycling	0.16
	Breakthrough experiment	Fresh bed-H_2O saturation	0.19
		Water pretreatment	0.75

The volumetric uptakes reported in Table 10 clearly indicate that RN2K outperforms RN2 under all the humid conditions evaluated. This is mainly ascribed to its higher packing density (0.39 g/cm^3). Moreover, an uptake of 0.75 mmol CO_2/cm^3 can be considered outstanding for a solid sorbent at 50 °C and a CO_2 partial pressure of ~14 kPa. Previous results reported for other adsorbents derived from pine sawdust (0.30 mmol CO_2/cm^3) [50] and spent coffee grounds (0.34 mmol CO_2/cm^3) [51] at 50 °C and CO_2 partial pressures of ~10 and 15 kPa, respectively, corroborate this statement.

3.4. CO_2 adsorption kinetics

To gain more insights on how the presence of water vapor can modify the kinetics of CO_2 adsorption on RN2 and RN2K, cycle I of the binary and ternary multicycle experiments have been assessed. Two kinetic models were considered: pseudo-first-order and Avrami´s fractional models.

Fig. 8 shows the q_t *vs.* t plots for RN2 and RN2K under dry and wet conditions together with the predictions from pseudo-first-order and Avrami´s models (Table 3).

Both carbons show two-stage adsorption that corresponds to mass transfer resistances to adsorption [52,53] and to proper surface adsorption that generally is very rapid [53–56].

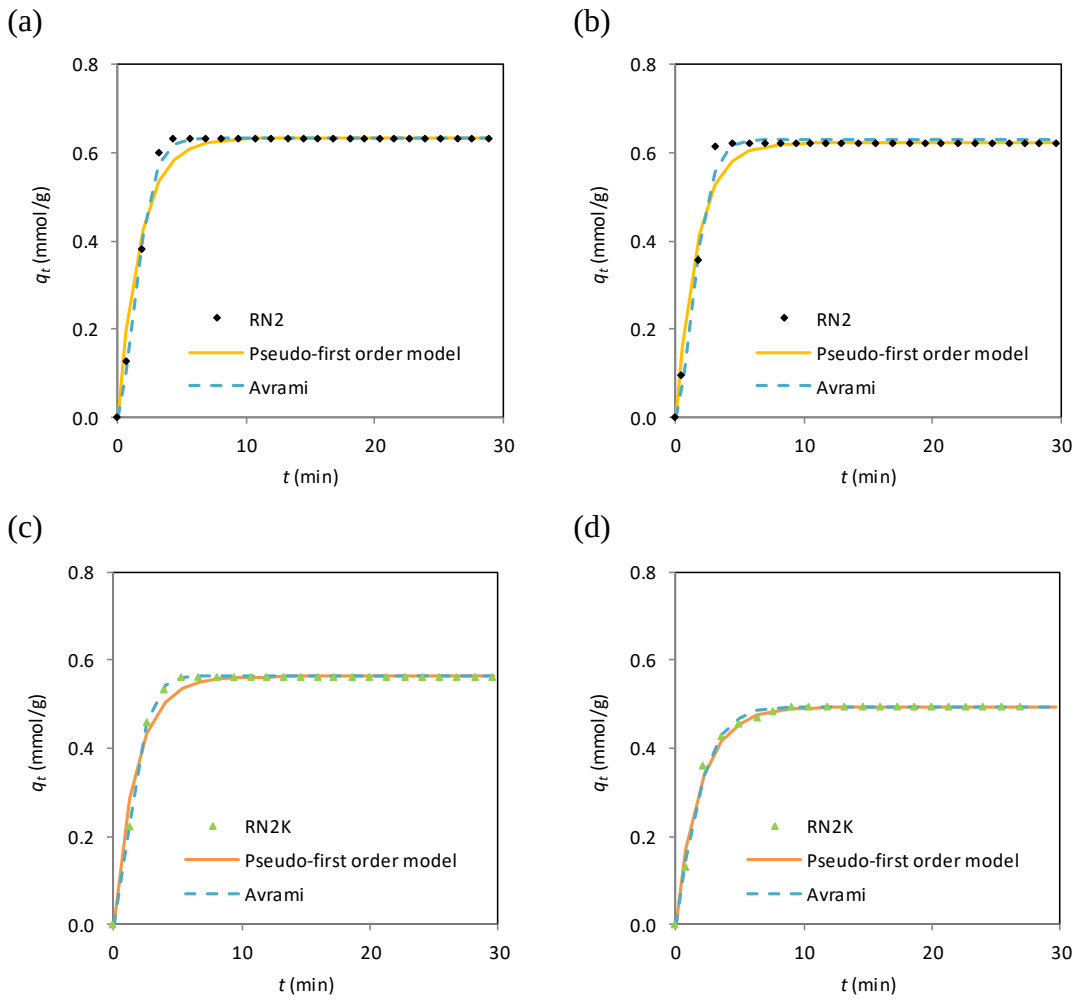

Fig. 8. Experimental and predicted q_t *vs.* t plots for RN2 and RN2K: binary experiments (a) and (c); ternary experiments (b) and (d)

The values of the kinetic parameters calculated for each model and the corresponding correlation coefficients (R^2) and associated sum of squared errors (SSE (%)) are listed in Table 11.

Table 11. Kinetic parameters of pseudo-first and Avrami models under the different adsorption conditions.

Sample	Experiment	Pseudo-first order			Avrami			
		k_f (min^{-1})	SSE (%)	R^2	k_A (min^{-1})	n_A	SSE (%)	R^2
RN2	CO_2/N_2	0.58	2.40	0.978	0.53	1.61	0.96	0.996
	$CO_2/N_2/H_2O$	0.61	2.60	0.974	0.55	1.77	1.28	0.993
RN2K	CO_2/N_2	0.57	1.69	0.983	0.53	1.62	0.18	1.000
	$CO_2/N_2/H_2O$	0.52	0.96	0.994	0.51	1.20	0.68	0.997

The pseudo-first-order model has certain limitations in fitting the CO_2 adsorption data on RN2 and RN2K, whilst Avrami's fractional order model suitably fits the experimental data from both binary and ternary experiments, and presents the lowest values of SSE (maximum of 1.28%) and values of R^2 close to unity. Therefore, compared with the pseudo-first order kinetic model, Avrami's equation seems the most accurate approach for describing CO_2 adsorption kinetics on the carbon adsorbents studied. This is in agreement with previous studies on the kinetics of CO_2 adsorption on biomass based carbons [28]. In the presence of moisture, Avrami´s exponent (n_A) for the support RN2 is higher due to longer contact time of the adsorbate with the adsorbent whilst under the same conditions this time is reduced for RN2K due to the existence of the hydration reaction represented in Eq. (2) [28,57–61]. This is consistent with values of the kinetic rate constants (k_A) that evidence the different adsorption rates as a function of the contact time [30].

The excellent quality of the fit of the Avrami's model to the experimental data at low and high surface coverage is most likely associated with its ability to account for complex reaction pathways [30,57,59]. Moreover, regarding the impregnated carbon RN2K, Serna-Guerrero et al. [57] also concluded that the best kinetic model for describing the CO_2 capture performance on amine-functionalized mesoporous silica was Avrami's equation.

3.5. CO_2 sorption kinetics: carbonation reaction

Since exponent (n_A) is a fractionary number and its result is attributed to multiple kinetic order of the adsorption procedure [58], and the kinetic rate constant (k_A) encompasses both chemical and physical adsorption [57], the Avrami model is unable to

explain thoroughly which sorption type is occurring and so does not account for the carbonation reaction mechanism. SCM is a dedicated model for heterogeneous reaction on solid particles and might better explain the carbonation reaction on the potassium carbonate based carbon sorbent.

In Section 3.2.3 it was concluded that RN2K is an excellent CO_2 sorbent when feeding a gas stream composed of 14% CO_2, 84% N_2 and 2% H_2O at 50 °C and atmospheric pressure while maintaining constant relative humidity (20%) in the bed. The CO_2 sorption capacity for RN2K at these conditions was 1.92 mmol/g (mass basis). Deducting the contribution from physical adsorption as estimated from the first cycle of the multicycle experiments under dry conditions (maximum capacity of 0.57 mmol/g) and considering complete conversion of K_2CO_3 to $KHCO_3$, the corresponding carbonation conversion (η) of RN2K could be estimated. A value of 45.5% was obtained at the end of the experiment (see Fig. 9).

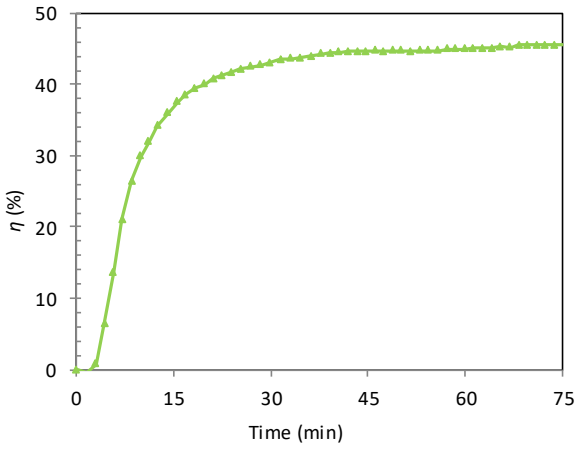

Fig. 9. Carbonation conversion of RN2K

The carbonation conversion increases up to 38.9% with a high reaction rate (in 17 min from the start of the experiment) and then increases an additional 6.6% at a much slower pace (over the following 51 min). Hence, a different mechanism of reaction can be anticipated for each region: surface chemical reaction control during the first 17 min and internal diffusion control for the remaining duration of the experiment. Fig. 10 plots the carbonation conversion functions and the corresponding fittings to the SCM. Data were fitted independently for the two regions.

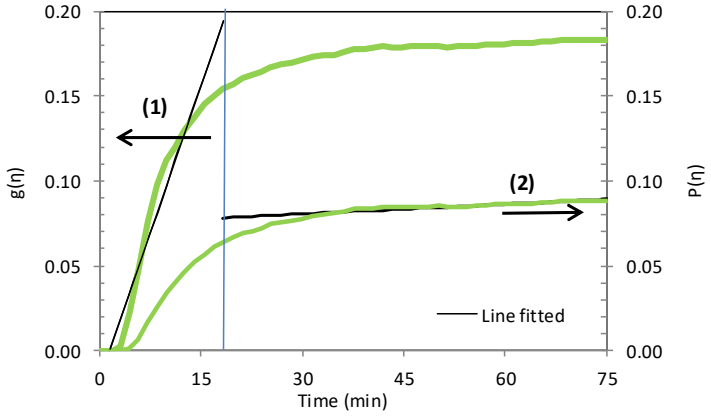

517 **Fig. 10.** Carbonation conversion of RN2K fitted to shrinking core model: (1) Surface
518 chemical reaction-controlled and (2) internal diffusion-controlled regions.

519 Kinetic parameters can be estimated from the slope and the intercept of the linear
520 fittings in both regions (See Table 5). Assuming a density of K_2CO_3 of 2.428 g/cm^3 [31],
521 a value of 1.76×10^{-2} mol/cm^3 is calculated for $C^0{}_{K_2CO_3}$. $C^0{}_{CO_2}$ and $C^0{}_{H_2O}$ are
522 5.3×10^{-6} mol/cm^3 and 9.4×10^{-7} mol/cm^3, respectively. The estimated parameters are
523 listed in Table 12.

524 **Table 12.** Kinetic parameters obtained from shrinking core model.

Surface chemical reaction-controlled region			Internal diffusion-controlled region		
$1/A_1$ (min^{-1})	k_s	r	$1/A_2$ (min^{-1})	D_e	r
1.16×10^{v2}	2.25×10^{7}	0.970	1.93×10^{-4}	6.27×10^{-5}	0.979

525 The shrinking core model provides a good fitting of the experimental results, thus
526 confirming the important contribution of carbonation reaction to CO_2 sorption on RN2K
527 under the conditions evaluated: 50ºC, atmospheric pressure, feed gas composition of 14%
528 CO_2, 84% N_2 and 2% H_2O and bed initially saturated in water (RH ≈ 20%). Since $1/A_1$ is
529 two order of magnitude greater than $1/A_2$, these results corroborate that the carbonation
530 conversion is mainly dependent on the first stage, the surface chemical reaction, which is
531 the fastest [31].
532

4. Conclusions

Potassium-based solid sorbent RN2K was prepared by impregnation with K_2CO_3 (40%) on activated carbon RN2, a microporous based biomass carbon produced in our laboratory. Impregnation of RN2 with potassium carbonate notably reduced the volume of available porosity for adsorption. The reduction of both the narrow pore size and the narrow micropore volume in RN2K caused a slight decrease in CO_2 uptake when physical adsorption was the single process involved. This was the case for the dry experiments feeding CO_2/N_2 and for the wet experiments feeding $CO_2/N_2/H_2O$ to a fresh bed of adsorbent. However, it was demonstrated that, independently of the H_2O concentration in the feed gas, a constant relative humidity of 20% in the RN2K bed promoted the carbonation reaction and boosted the CO_2 sorption capacity up to approximately 2 mmol/g at 50 °C and 14 kPa partial pressure of CO_2. In addition, RN2K showed outstanding performance on a volumetric basis due to its higher packing density.

The kinetics of CO_2 sorption on RN2K where studied from two approaches: one focused on physical adsorption and the other one on the carbonation reaction. Avrami's and Shrinking Core models suitably fitted the experimental data in each of the two cases. CO_2 adsorption on RN2K is however faster than carbonation.

RN2K showed stable performance upon cycling in a fixed-bed set-up and enhanced CO_2 capture capacity under the evaluated conditions. However, there is a trade-off between capture capacity and sorption kinetics for the potassium carbonate based carbon sorbent: carbonation leads to high capacity at the expense of slower kinetics whereas physical adsorption proceeds faster but reaches significantly lower uptakes. This opens the path for the tailoring of this material according to the process configuration design (rapid or slow cycling) and to the targets in CO_2 capture (CO_2 recovery and purity). Cycles with longer adsorption step will allow RN2K to go through carbonation reaction and so attain higher CO_2 uptakes; however, regeneration over extended time will lead to higher CO_2 recovery but lower purity.

Acknowledgments: N.Q. acknowledges a fellowship from the Gobierno del Principado de Asturias (Programa Severo Ochoa).

5. References

[1] H.A. Patel, J. Byun, C.T. Yavuz, ChemSusChem 10 (2017) 1303–1317.

[2] J.B. Lee, T.H. Eom, B.S. Oh, J.I. Baek, J. Ryu, W.S. Jeon, Y.H. Wi, C.K. Ryu, Energy Procedia 4 (2011) 1494–1499.

[3] A. Jayakumar, A. Gomez, N. Mahinpey, Appl. Energy 179 (2016) 531–543.

[4] M. Wang, A. Lawal, P. Stephenson, J. Sidders, C. Ramshaw, Chem. Eng. Res. Des. 89 (2011) 1609–1624.

[5] A.G. Okunev, V.E. Sharonov, A. V. Gubar", I.G. Danilova, E.A. Paukshtis, E.M. Moroz, T.A. Kriger, V. V. Malakhov, Y.I. Aristov, Russ. Chem. Bull. 52 (2003) 359–363.

[6] C. Zhao, C. Zhao, X. Chen, E.J. Anthony, X. Jiang, L. Duan, Y. Wu, W. Dong, Prog. Energy Combust. Sci. 39 (2013) 515–534.

[7] J. V. Veselovskaya, V.S. Derevschikov, T.Y. Kardash, O.A. Stonkus, T.A. Trubitsina, A.G. Okunev, Int. J. Greenh. Gas Control 17 (2013) 332–340.

[8] H. Hayashi, J. Taniuchi, N. Furuyashiki, S. Sugiyama, S. Hirano, N. Shigemoto, T. Nonaka, Ind. Eng. Chem. Res. 37 (1998) 185–191.

[9] Y. Guo, C. Li, S. Lu, C. Zhao, Energy & Fuels 29 (2015) 8151–8156.

[10] C. Qin, J. Yin, J. Ran, L. Zhang, B. Feng, Appl. Energy 136 (2014) 280–288.

[11] C. Zhao, Y. Guo, C. Li, S. Lu, Chem. Eng. J. 254 (2014) 524–530.

[12] N. Querejeta, M. Plaza, F. Rubiera, C. Pevida, Materials (Basel). 9 (2016) 359.

[13] Y. Guo, C. Zhao, C. Li, Chem. Eng. Technol. 38 (2015) 891–899.

[14] S. Brunauer, P.H. Emmett, E. Teller, J. Am. Chem. Soc. 60 (1938) 309–319.

[15] F. Stoeckli, Russ. Chem. Bull. 50 (n.d.) 2265–2272.

[16] H.F. Stoeckli, Carbon N. Y. 19 (1981) 325–326.

[17] F. Stoeckli, L. Ballerini, Fuel 70 (1991) 557–559.

[18] M.V. Gil, N. Álvarez-Gutiérrez, M. Martínez, F. Rubiera, C. Pevida, A. Morán, Chem. Eng. J. 269 (2015) 148–158.

[19] M.G. Plaza, I. Durán, N. Querejeta, F. Rubiera, C. Pevida, Ind. Eng. Chem. Res. 55 (2016) 3097–3112.

[20] M.G. Plaza, I. Durán, N. Querejeta, F. Rubiera, C. Pevida, Ind. Eng. Chem. Res. 55 (2016) 6854–6865.

[21] N. Álvarez-Gutiérrez, S. García, M.V. Gil, F. Rubiera, C. Pevida, Energy & Fuels 30 (2016) 5005–5015.

[22] N. Álvarez-Gutiérrez, M. V. Gil, F. Rubiera, C. Pevida, Fuel Process. Technol. 142

(2016) 361–369.
[23] I. Durán, F. Rubiera, C. Pevida, Energies 10 (2017) 827.
[24] S.C. Lee, B.Y. Choi, C.K. Ryu, Y.S. Ahn, T.J. Lee, J.C. Kim, Korean J. Chem. Eng. 23 (2006) 374–379.
[25] Y. Guo, C. Zhao, C. Li, Y. Wu, Chem. Eng. J. 260 (2015) 596–604.
[26] S.C. Lee, H.J. Chae, B.Y. Choi, S.Y. Jung, C.Y. Ryu, J.J. Park, J.-I. Baek, C.K. Ryu, J.C. Kim, Korean J. Chem. Eng. 28 (2011) 480–486.
[27] L. Stevens, K. Williams, W.Y. Han, T. Drage, C. Snape, J. Wood, J. Wang, Chem. Eng. J. 215–216 (2013) 699–708.
[28] N. Álvarez-Gutiérrez, M. V. Gil, F. Rubiera, C. Pevida, Chem. Eng. J. 307 (2017) 249–257.
[29] S. Lagergren, Handlingar 24 (1898) 1–39.
[30] E.C.N. Lopes, F.S.C. dos Anjos, E.F.S. Vieira, A.R. Cestari, J. Colloid Interface Sci. 263 (2003) 542–547.
[31] C. Zhao, X. Chen, C. Zhao, Ind. Eng. Chem. Res. 51 (2012) 14361–14366.
[32] P.K. Gbor, C.Q. Jia, Chem. Eng. Sci. 59 (2004) 1979–1987.
[33] N. Querejeta, M.V. Gil, C. Pevida, T.A. Centeno, J. CO2 Util. 26 (2018) 1–7.
[34] H. Wei, S. Deng, B. Hu, Z. Chen, B. Wang, J. Huang, G. Yu, ChemSusChem 5 (2012) 2354–2360.
[35] Z. Zhang, J. Zhou, W. Xing, Q. Xue, Z. Yan, S. Zhuo, S.Z. Qiao, Phys. Chem. Chem. Phys. 15 (2013) 2523.
[36] J. Serafin, U. Narkiewicz, A.W. Morawski, R.J. Wróbel, B. Michalkiewicz, J. CO2 Util. 18 (2017) 73–79.
[37] J.P. Marco-Lozar, M. Kunowsky, F. Suárez-García, A. Linares-Solano, Carbon N. Y. 72 (2014) 125–134.
[38] B. Adeniran, E. Masika, R. Mokaya, J. Mater. Chem. A 2 (2014) 14696.
[39] H. Luo, H. Chioyama, S. Thürmer, T. Ohba, H. Kanoh, Energy & Fuels 29 (2015) 4472–4478.
[40] C. Zhao, X. Chen, C. Zhao, Energy & Fuels 26 (2012) 1401–1405.
[41] C. Zhao, X. Chen, C. Zhao, Ind. Eng. Chem. Res. 49 (2010) 12212–12216.
[42] S. Freguia, G.T. Rochelle, AIChE J. 49 (2003) 1676–1686.
[43] T. Neveux, Y. Le Moullec, J.P. Corriou, E. Favre, Chem. Eng. Trans. 35 (2013) 337–342.
[44] G. Puxty, R. Rowland, A. Allport, Q. Yang, M. Bown, R. Burns, M. Maeder, M.

631 Attalla, Environ. Sci. Technol. 43 (2009) 6427–6433.
632 [45] L. Dubois, D. Thomas, Chem. Eng. Technol. 35 (2012) 513–524.
633 [46] S.C. Lee, J.C. Kim, Catal. Surv. from Asia 11 (2007) 171–185.
634 [47] S.C. Lee, B.Y. Choi, T.J. Lee, C.K. Ryu, Y.S. Ahn, J.C. Kim, Catal. Today 111
635 (2006) 385–390.
636 [48] Y. Guo, C. Li, S. Lu, C. Zhao, Chem. Eng. J. 301 (2016) 325–333.
637 [49] Y. Guo, C. Li, S. Lu, C. Zhao, Chem. Eng. J. 308 (2017) 516–526.
638 [50] I. Durán, F. Rubiera, C. Pevida, J. CO2 Util. 26 (2018) 454–464.
639 [51] M.G. Plaza, A.S. González, C. Pevida, F. Rubiera, Fuel 140 (2015) 633–648.
640 [52] D.D. Do, H.D. Do, Sep. Purif. Technol. 20 (2000) 49–65.
641 [53] G. Song, X. Zhu, R. Chen, Q. Liao, Y.-D. Ding, L. Chen, Chem. Eng. J. 283 (2016)
642 175–183.
643 [54] B.H. Hameed, I.A.W. Tan, A.L. Ahmad, Chem. Eng. J. 144 (2008) 235–244.
644 [55] L. Ai, M. Li, L. Li, J. Chem. Eng. Data 56 (2011) 3475–3483.
645 [56] M.H. Kalavathy, T. Karthikeyan, S. Rajgopal, L.R. Miranda, J. Colloid Interface
646 Sci. 292 (2005) 354–362.
647 [57] R. Serna-Guerrero, A. Sayari, Chem. Eng. J. 161 (2010) 182–190.
648 [58] B. Royer, N.F. Cardoso, E.C. Lima, J.C.P. Vaghetti, N.M. Simon, T. Calvete, R.C.
649 Veses, J. Hazard. Mater. 164 (2009) 1213–1222.
650 [59] A.R. Cestari, E.F.S.S. Vieira, G.S. Vieira, L.E. Almeida, J. Hazard. Mater. 138
651 (2006) 133–141.
652 [60] A.R. Cestari, E.F.S. Vieira, J.D.S. Matos, D.S.C. Dos Anjos, J. Colloid Interface
653 Sci. 285 (2005) 288–295.
654 [61] E.W. de Menezes, E.C. Lima, B. Royer, F.E. de Souza, B.D. dos Santos, J.R.
655 Gregório, T.M.H. Costa, Y. Gushikem, E. V. Benvenutti, J. Colloid Interface Sci.
656 378 (2012) 10–20.
657
658

659 Graphical abstract

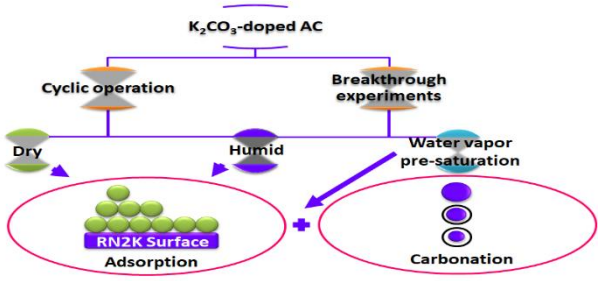

660 K_2CO_3 doped biomass-based AC is a promising candidate for CO_2 capture at low
661 temperature (50 °C) under humid flue gas conditions. The use of a biocarbon as support
662 constitutes a sustainable and low-cost approach.

663